Investigation of combined Brillouin gain and loss in a birefringent fiber with applications in sensing

Daisy Williams, Xiaoyi Bao, Liang Chen

Department of Physics, University of Ottawa, Ottawa, ON, K1N 6N5, Canada
Corresponding author: dwill087@uottawa.ca

Received July 3, 2014; accepted September 11, 2014; posted online November 17, 2014

The most general model of elliptical birefringence in an optical fiber is extended to describe a transient Brillouin interaction including both gain and loss. The effects of elliptical birefringence cause a Brillouin spectral shape distortion, which is detrimental for fiber sensing techniques. The model investigates the effects of birefringence and the corresponding evolution of spectral distortion effects along the fiber, and also investigates regimes where this distortion is minimal.

OCIS codes: 310.5448, 290.5900, 290.5830, 190.4370.
doi: 10.3788/COL201412.123101.

Birefringence is the optical property of a material having a refractive index which depends on the polarization and propagation direction of light[1,2]. In optical fibers, the birefringence effect is detrimental for a variety of reasons, among which the Brillouin gain depends on the state of polarization in the fiber[3–7] and unintended birefringence causes the polarization of the optical field to change during propagation through the fiber. The local refractive index changes associated with density fluctuations changes the shape of Brillouin spectrum, causing errors in distributed temperature and strain measurement[6–11].

Currently, there exist works which have investigated the polarization effects on stimulated Brillouin scattering (SBS) in optical fibers[3,5,7,12] which have shown that the Stokes gain is strongly dependent on polarization effects. In Ref. [13], a vector formalism was used to characterize the effects of birefringence on the SBS interaction; however, only linearly polarized pump wave (PW) and signal wave were investigated, for which an undepleted pump regime was assumed. The abovementioned works[5,7,12,13] also treat a steady-state SBS system where both the PW and Stokes wave (SW) are continuous. Additionally, none of these references investigated the effect of birefringence and polarization effects on the spectral distortion. In Ref. [4], though pulse length was taken into account, Brillouin spectrum distortion was not considered. More importantly, the impact of the nonlinear effect under different pump powers convoluted with the fiber birefringence and its impact on the Brillouin spectrum shape and peak shift have not been examined yet. None of the aforementioned works took into consideration the most general case of birefringence, which is elliptical birefringence, or the effects of this birefringence on the combined Brillouin gain and loss regime in an optical fiber.

A more accurate model of the polarization-dependent Brillouin gain and loss interaction, which includes the case of elliptical birefringence is needed. The model presented here describes the most comprehensive equations considering the birefringence effects in an optical fiber. Being an extension of the work presented in Ref. [14], which described the SBS interaction in a birefringent fiber, this model includes the most general case of elliptical birefringence, the effects of polarization mode dispersion (PMD), polarization-dependent loss (PDL), phonon resonance structures, pulse length, as well as the overall attenuation of the fiber.

For sensing applications involving optical differential parametric amplification in Brillouin optical time domain analysis (ODPA-BOTDA) systems[10,11], which employ both SW and anti-SW (ASW) pulses, this investigation of the effects of birefringence on the combined Brillouin gain and loss is paramount. Additionally, since spectral distortion is detrimental in sensing applications, it is important to investigate a power regime in which birefringence effects are minimal.

The process of Brillouin gain and loss is studied in a birefringent polarization-maintaining optical fiber, with a core radius of 4.1 μm. The configuration comprises a PW launched from one end, and a SW and an ASW launched from the other end. The PW, SW, and ASW have x- and y- eigen-polarization components. The schematic arrangement is shown in Fig. 1.

The extended system of Eqs. (1)–(6) describes the interaction of the PW, SW, and ASW (Fig. 1) including the effects of PMD and PDL, similar to the system presented in Ref. [14]. Other than the usual slowly varying amplitude approximation, the only additional

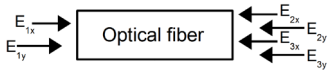

Fig. 1. Schematic arrangement of SBS in an optical fiber of length L. E_{1x} and E_{1y}, PWs; E_{2x} and E_{2y}, SWs; E_{3x} and E_{3y}, ASWs.

approximation in establishing Eqs. (1)–(6) is the assumption that the phonon fields are established almost simultaneously, which is not a bad approximation for the majority of practical cases[1,15].

$$\begin{aligned}
&\frac{\partial \mathrm{E}_{1x}}{\partial z}+\frac{\overline{n}_1}{c}\frac{\partial \mathrm{E}_{1x}}{\partial t}+\left(\overline{\alpha}_1+\frac{\Delta\overline{\alpha}_1}{2}+\mathrm{i}\frac{\Delta\overline{n}_1\omega_1}{2c}\right)\mathrm{E}_{1x}\\
&=\left.\begin{aligned}
&\mathrm{i}\frac{\gamma_e^2\omega_1^2}{2_0c^2v}\frac{1}{\left(\Omega_{\mathrm{B}xx}^{\mathrm{SW}}-\Omega_1\right)-\mathrm{i}\dfrac{\Gamma_\mathrm{B}}{2}}\\
&\mathrm{E}_{1x}\mathrm{E}_{2x}^{*}\mathrm{E}_{2x}\frac{1}{2}\left(1+\mathrm{S}_{x1}\cdot\mathrm{S}_{x2}\right)\\
&+\mathrm{i}\frac{\gamma_e^2\omega_1^2}{2_0c^2v}\frac{1}{\left(\Omega_{\mathrm{B}xy}^{\mathrm{SW}}-\Omega_1\right)-\mathrm{i}\dfrac{\Gamma_\mathrm{B}}{2}}\\
&\mathrm{E}_{1x}\mathrm{E}_{2y}^{*}\mathrm{E}_{2y}\frac{1}{2}\left(1+\mathrm{S}_{x1}\cdot\mathrm{S}_{y2}\right)
\end{aligned}\right\}\text{Stokes}\\
&\left.\begin{aligned}
&+\mathrm{i}\frac{\gamma_\mathrm{e}^2\omega_1^2}{2\rho_0c^2v}\frac{1}{\left(\Omega_{\mathrm{B}xx}^{\mathrm{ASW}}-\Omega_2\right)-\mathrm{i}\dfrac{\Gamma_\mathrm{B}}{2}}\\
&\mathrm{E}_{1x}\mathrm{E}_{3x}^{*}\mathrm{E}_{3x}\frac{1}{2}\left(1+\mathbf{S}_{x1}\cdot\mathbf{S}_{x3}\right)\\
&+\mathrm{i}\frac{\gamma_\mathrm{e}^2\omega_1^2}{2\rho_0c^2v}\frac{1}{\left(\Omega_{\mathrm{B}xy}^{\mathrm{ASW}}-\Omega_2\right)-\mathrm{i}\dfrac{\Gamma_\mathrm{B}}{2}}\\
&\mathrm{E}_{1x}\mathrm{E}_{3y}^{*}\mathrm{E}_{3y}\frac{1}{2}\left(1+\mathbf{S}_{x1}\cdot\mathbf{S}_{y3}\right),
\end{aligned}\right\}\text{anti-Stokes}
\end{aligned}\tag{1}$$

$$\begin{aligned}
&\frac{\partial \mathrm{E}_{1y}}{\partial z}+\frac{\overline{n}_1}{c}\frac{\partial \mathrm{E}_{1y}}{\partial t}+\left(\overline{\alpha}_1-\frac{\Delta\overline{\alpha}_1}{2}-\mathrm{i}\frac{\Delta\overline{n}_1\omega_1}{2c}\right)\mathrm{E}_{1y}\\
&=\left.\begin{aligned}
&\mathrm{i}\frac{\gamma_\mathrm{e}^2\omega_1^2}{2\rho_0c^2v}\frac{1}{\left(\Omega_{\mathrm{B}yy}^{\mathrm{SW}}-\Omega_1\right)-\mathrm{i}\dfrac{\Gamma_\mathrm{B}}{2}}\\
&\mathrm{E}_{1y}\mathrm{E}_{2y}^{*}\mathrm{E}_{2y}\frac{1}{2}\left(1+\mathbf{S}_{y1}\cdot\mathbf{S}_{y2}\right)\\
&+\mathrm{i}\frac{\gamma_\mathrm{e}^2\omega_1^2}{2\rho_0c^2v}\frac{1}{\left(\Omega_{\mathrm{B}yx}^{\mathrm{SW}}-\Omega_1\right)-\mathrm{i}\dfrac{\Gamma_\mathrm{B}}{2}}\\
&\mathrm{E}_{1y}\mathrm{E}_{2x}^{*}\mathrm{E}_{2x}\frac{1}{2}\left(1+\mathbf{S}_{y1}\cdot\mathbf{S}_{x2}\right)
\end{aligned}\right\}\text{Stokes}\\
&\left.\begin{aligned}
&+\mathrm{i}\frac{\gamma_\mathrm{e}^2\omega_1^2}{2\rho_0c^2v}\frac{1}{\left(\Omega_{\mathrm{B}yy}^{\mathrm{ASW}}-\Omega_2\right)-\mathrm{i}\dfrac{\Gamma_\mathrm{B}}{2}}\\
&\mathrm{E}_{1y}\mathrm{E}_{3y}^{*}\mathrm{E}_{3y}\frac{1}{2}\left(1+\mathbf{S}_{y1}\cdot\mathbf{S}_{y3}\right)\\
&+\mathrm{i}\frac{\gamma_\mathrm{e}^2\omega_1^2}{2\rho_0c^2v}\frac{1}{\left(\Omega_{\mathrm{B}yx}^{\mathrm{ASW}}-\Omega_2\right)-\mathrm{i}\dfrac{\Gamma_\mathrm{B}}{2}}\\
&\mathrm{E}_{1y}\mathrm{E}_{3x}^{*}\mathrm{E}_{3x}\frac{1}{2}\left(1+\mathbf{S}_{y1}\cdot\mathbf{S}_{x3}\right),
\end{aligned}\right\}\text{anti-Stokes}
\end{aligned}\tag{2}$$

$$\begin{aligned}
&-\frac{\partial \mathrm{E}_{2x}}{\partial z}+\frac{\overline{n}_2}{c}\frac{\partial \mathrm{E}_{2x}}{\partial t}+\left(\overline{\alpha}_2+\frac{\Delta\overline{\alpha}_2}{2}+\mathrm{i}\frac{\Delta\overline{n}_2\omega_2}{2c}\right)\mathrm{E}_{2x}\\
&=\mathrm{i}\frac{\gamma_\mathrm{e}^2\omega_2^2}{2\rho_0c^2v}\frac{1}{\left(\Omega_{\mathrm{B}xx}^{\mathrm{SW}}-\Omega_1\right)-\mathrm{i}\dfrac{\Gamma_\mathrm{B}}{2}}\mathrm{E}_{2x}\mathrm{E}_{1x}^{*}\mathrm{E}_{1x}\frac{1}{2}\left(1+\mathbf{S}_{x1}\cdot\mathbf{S}_{x2}\right)\\
&+\mathrm{i}\frac{\gamma_\mathrm{e}^2\omega_2^2}{2\rho_0c^2v}\frac{1}{\left(\Omega_{\mathrm{B}yx}^{\mathrm{SW}}-\Omega_1\right)-\mathrm{i}\dfrac{\Gamma_\mathrm{B}}{2}}\mathrm{E}_{2x}\mathrm{E}_{1y}^{*}E_{1y}\frac{1}{2}\left(1+\mathbf{S}_{y1}\cdot\mathbf{S}_{x2}\right),
\end{aligned}\tag{3}$$

$$\begin{aligned}
&-\frac{\partial \mathrm{E}_{2y}}{\partial z}+\frac{\overline{n}_2}{c}\frac{\partial \mathrm{E}_{2y}}{\partial t}+\left(\overline{\alpha}_2-\frac{\Delta\overline{\alpha}_2}{2}-\mathrm{i}\frac{\Delta\overline{n}_2\omega_2}{2\mathrm{c}}\right)\mathrm{E}_{2y}\\
&=\mathrm{i}\frac{\gamma_\mathrm{e}^2\omega_2^2}{2\rho_0c^2v}\frac{1}{\left(\Omega_{\mathrm{B}yy}^{\mathrm{SW}}-\Omega_1\right)-\mathrm{i}\dfrac{\Gamma_\mathrm{B}}{2}}\mathrm{E}_{2y}\mathrm{E}_{1y}^{*}\mathrm{E}_{1y}\frac{1}{2}\left(1+\mathbf{S}_{y1}\cdot\mathbf{S}_{y2}\right)\\
&+\mathrm{i}\frac{\gamma_\mathrm{e}^2\omega_2^2}{2\rho_0c^2v}\frac{1}{\left(\Omega_{\mathrm{B}xy}^{\mathrm{SW}}-\Omega_1\right)-\mathrm{i}\dfrac{\Gamma_\mathrm{B}}{2}}\mathrm{E}_{2y}\mathrm{E}_{1x}^{*}\mathrm{E}_{1x}\frac{1}{2}\left(1+\mathbf{S}_{x1}\cdot\mathbf{S}_{y2}\right),
\end{aligned}\tag{4}$$

$$\begin{aligned}
&-\frac{\partial \mathrm{E}_{3x}}{\partial z}+\frac{\overline{n}_3}{c}\frac{\partial \mathrm{E}_{3x}}{\partial t}+\left(\overline{\alpha}_3+\frac{\Delta\overline{\alpha}_3}{2}+\mathrm{i}\frac{\Delta\overline{n}_3\omega_3}{2c}\right)\mathrm{E}_{3x}\\
&=\mathrm{i}\frac{\gamma_\mathrm{e}^2\omega_3^2}{2\rho_0c^2v}\frac{1}{\left(\Omega_{\mathrm{B}xx}^{\mathrm{ASW}}-\Omega_2\right)-\mathrm{i}\dfrac{\Gamma_\mathrm{B}}{2}}\mathrm{E}_{3x}\mathrm{E}_{1x}^{*}\mathrm{E}_{1x}\frac{1}{2}\left(1+\mathbf{S}_{x1}\cdot\mathbf{S}_{x3}\right)\\
&+\mathrm{i}\frac{\gamma_\mathrm{e}^2\omega_2^2}{2\rho_0c^2v}\frac{1}{\left(\Omega_{\mathrm{B}yx}^{\mathrm{ASW}}-\Omega_2\right)-\mathrm{i}\dfrac{\Gamma_\mathrm{B}}{2}}\mathrm{E}_{3x}\mathrm{E}_{1y}^{*}\mathrm{E}_{1y}\frac{1}{2}\left(1+\mathbf{S}_{y1}\cdot\mathbf{S}_{x3}\right),
\end{aligned}\tag{5}$$

$$\begin{aligned}
&-\frac{\partial \mathrm{E}_{3y}}{\partial z}+\frac{\overline{n}_3}{c}\frac{\partial \mathrm{E}_{3y}}{\partial t}+\left(\overline{\alpha}_3-\frac{\Delta\overline{\alpha}_3}{2}-\mathrm{i}\frac{\Delta\overline{n}_3\omega_3}{2c}\right)\mathrm{E}_{3y}\\
&=\mathrm{i}\frac{\gamma_\mathrm{e}^2\omega_3^2}{2\rho_0c^2v}\frac{1}{\left(\Omega_{\mathrm{B}yy}^{\mathrm{ASW}}-\Omega_2\right)-\mathrm{i}\dfrac{\Gamma_\mathrm{B}}{2}}\mathrm{E}_{3y}\mathrm{E}_{1y}^{*}\mathrm{E}_{1y}\frac{1}{2}\left(1+\mathbf{S}_{y1}\cdot\mathbf{S}_{y3}\right)\\
&+\mathrm{i}\frac{\gamma_\mathrm{e}^2\omega_2^2}{2\rho_0c^2v}\frac{1}{\left(\Omega_{\mathrm{B}xy}^{\mathrm{ASW}}-\Omega_2\right)-\mathrm{i}\dfrac{\Gamma_\mathrm{B}}{2}}\mathrm{E}_{3y}\mathrm{E}_{1x}^{*}\mathrm{E}_{1x}\frac{1}{2}\left(1+\mathbf{S}_{x1}\cdot\mathbf{S}_{y3}\right).
\end{aligned}\tag{6}$$

For the SW, we have $\Omega^{\mathrm{SW}}{}_{\mathrm{B}xx}=(v/c)(n_{1x}\omega_1+n_{2x}\omega_2)$, $\Omega^{\mathrm{SW}}{}_{\mathrm{B}yy}=(v/c)(n_{1y}\omega_1+n_{2y}\omega_2)$, $\Omega^{\mathrm{SW}}{}_{\mathrm{B}xy}=(v/c)(n_{1x}\omega_1+n_{2y}\omega_2)$, $\Omega^{\mathrm{SW}}{}_{\mathrm{B}yx}=(v/c)(n_{1y}\omega_1+n_{2x}\omega_2)$, and for the ASW we have $\Omega^{\mathrm{ASW}}{}_{\mathrm{B}xx}=(v/c)(n_{1x}\omega_1+n_{3x}\omega_2)$, $\Omega^{\mathrm{ASW}}{}_{\mathrm{B}yy}=(v/c)(n_{1y}\omega_1+n_{3y}\omega_2)$, $\Omega^{\mathrm{ASW}}{}_{\mathrm{B}xy}=(v/c)(n_{1x}\omega_1+n_{3y}\omega_2)$, $\Omega^{\mathrm{ASW}}{}_{\mathrm{B}yx}=(v/c)(n_{1y}\omega_1+n_{3x}\omega_2)$, which are the Brillouin frequencies associated with the principal axes beatings[6], where ω_1 is the angular frequency of the PW, and ω_2 and ω_3 are the angular frequencies of the SW and ASW, respectively. n_{ij}, $i=1, 2, 3$, $j=x, y$, are the indices of refraction associated with the principal axes of the PW, SW, and ASW, respectively. $\Omega_1=\omega_1-\omega_2$ is the angular frequency of the AW_1 caused

by the interaction of the PW and SW, and $\Omega_2 = \omega_3 - \omega_1$ is the angular frequency of the AW_2 caused by the interaction of the PW and ASW. E_{ij}, $i = 1, 2, 3$, $j = x, y$, are the complex amplitudes of the PW, SW, and the ASW, respectively. c is the speed of light, ρ_0 is the mean density of the fiber, γ_e is the electrostrictive constant, z is the coordinate along the fiber, v is the speed of sound in the fiber, Γ_B is the Brillouin linewidth, and finally, α_{ij}, $i = 1, 2, 3$, $j = x, y$, represent the fiber attenuations of the principal axes of polarization of the three interacting waves.

$\mathbf{S}_{1x}$, $\mathbf{S}_{1y}$, $\mathbf{S}_{2x}$, $\mathbf{S}_{2y}$, $\mathbf{S}_{3x}$, and $\mathbf{S}_{3y}$ represent the Stokes vectors in the Poincaré sphere polarization representation[16,17], and are used to define the polarization of the propagating lights[2,14,16,17]. In this case, if $\mathbf{S}_{x1}$ is defined as $\mathbf{S}_{x1} = (a, b, c)$, then $\mathbf{S}_{y1} = (-a, -b, -c)$, $\mathbf{S}_{x2} = (a, b, -c)$, $\mathbf{S}_{y2} = (-a, -b, c)$, $\mathbf{S}_{x3} = (a, b, -c)$, and $\mathbf{S}_{y3} = (-a, -b, c)$, where a, b, and c are the Stokes vector components normalized such that $a^2 + b^2 + c^2 = 1$. From this arrangement it is apparent that for fibers having elliptical birefringence ($0 < |c| < 1$), the most general beating situation will be excited.

The remaining simplification included making the birefringence effect more explicit, jutstified by the fact that birefringence and PDL are both small. It is defined that $\overline{n_i} = (n_{ix} + n_{iy})/2$, $\Delta\overline{n_i} = n_{ix} - n_{iy}$, $\overline{\alpha_i} = (\alpha_{ix} + \alpha_{iy})/2$, $\Delta\overline{\alpha_i} = \alpha_{ix} - \alpha_{iy}$, $i = 1, 2, 3$.

In the above arrangement, the PW input parameters are known only at the beginning of the fiber, that is, at $z = 0$. Correspondingly, the SW and ASW input parameters are known only at the end of the fiber, that is, at $z = L$, where L is the length of the fiber. Therefore, the boundary conditions for the system of Eqs. (1)–(6) are similar to previously studied configurations with one pulse[6,18,19]. The conditions for two pulses are as follows: $|E_{ij}(0)|^2 = E^2_{ij0}$, $i = 1, 2, 3$, $j = x, y$, where E^2_{ij0} are the known squared absolute values of the complex fields E_{1j}, respectively. In Eqs. (1)–(6), we have employed the dimensionless length variable $\ell = z / L$, and the dimensionless time variable $\tau = t / t_c$, where $t_c = L \cdot n_{avg}/c$ is the transit time and n_{avg} is the average index of refraction. The dimensionless intensity variables are defined as the ratio of powers: $Y_{ij} = P_{ij}/P_{ij0}$, $i = 1, 2, 3$, $j = x, y$. Additionally, ε_{ij} are the dimensionless loss terms, defined as $\varepsilon_{ij} = 2L\alpha_{ij}$, $i = 1, 2, 3$, $j = x, y$. The form factor component of the β–coefficients is defined as $\xi_{ij}^{SW} = (\Omega_{Bij} - \Omega_1)/(\Gamma_B/2)$ or $\xi_{ij}^{ASW} = (\Omega_{Bij} - \Omega_2)/(\Gamma_B/2)$, where $i = x, y$ and $j = x, y$. The method of characteristics was employed as in Refs. [2,14,20,21] and the following change of variables was used: $u = (1/\overline{n})\tau + l$ and $v = (1/\overline{n})\tau - l$, where the approximation $\overline{n}_1 \approx \overline{n}_2 = \overline{n}$ was employed. The resulting system of equations is as follows, with β–coefficients as defined by

$$\frac{dY_{1x}}{du} = -\underbrace{\left[\beta_{1a}Y_{2x} + \beta_{1b}Y_{2y}\right]Y_{1x}}_{\text{Stokes}} + \underbrace{\left[\beta_{2a}Y_{3x} + \beta_{2b}Y_{3y}\right]Y_{1x}}_{\text{anti-Stokes}} - \varepsilon_{1x}Y_{1x}, \tag{7}$$

$$\frac{dY_{1y}}{du} = -\underbrace{\left[\beta_{1c}Y_{2y} + \beta_{1d}Y_{2x}\right]Y_{1y}}_{\text{Stokes}} + \underbrace{\left[\beta_{2c}Y_{3y} + \beta_{2d}Y_{3x}\right]Y_{1y}}_{\text{anti-Stokes}} - \varepsilon_{1y}Y_{1y}, \tag{8}$$

$$\frac{dY_{2x}}{dv} = \left[\beta_{3a}Y_{1x} + \beta_{3b}Y_{1y}\right]Y_{2x} - \varepsilon_{2x}Y_{2x}, \tag{9}$$

$$\frac{dY_{2y}}{dv} = \left[\beta_{3c}Y_{1y} + \beta_{3d}Y_{1x}\right]Y_{2y} - \varepsilon_{2y}Y_{2y}, \tag{10}$$

$$\frac{dY_{3x}}{dv} = -\left[\beta_{4a}Y_{1x} + \beta_{4b}Y_{1y}\right]Y_{3x} - \varepsilon_{3x}Y_{3x}, \tag{11}$$

$$\frac{dY_{3y}}{dv} = -\left[\beta_{4c}Y_{1y} + \beta_{4d}Y_{1x}\right]Y_{3y} - \varepsilon_{3y}Y_{3y}, \tag{12}$$

$$\beta_{1a} = \frac{4\gamma_e^2 k^2 P_{2x0} L}{r^2 \overline{n}_2 \rho_0 c v \Gamma_B} \cdot \frac{1}{2} \frac{1 + \mathbf{S}_{x1} \cdot \mathbf{S}_{x2}}{1 + \left(\xi_{xx}^{SW}\right)^2}, \tag{13}$$

$$\beta_{1b} = \frac{4\gamma_e^2 k^2 P_{2y0} L}{r^2 \overline{n}_2 \rho_0 c v \Gamma_B} \cdot \frac{1}{2} \frac{1 + \mathbf{S}_{x1} \cdot \mathbf{S}_{y2}}{1 + \left(\xi_{xy}^{SW}\right)^2}, \tag{14}$$

$$\beta_{1c} = \frac{4\gamma_e^2 k^2 P_{2y0} L}{r^2 \overline{n}_2 \rho_0 c v \Gamma_B} \cdot \frac{1}{2} \frac{1 + \mathbf{S}_{y1} \cdot \mathbf{S}_{y2}}{1 + \left(\xi_{yy}^{SW}\right)^2}, \tag{15}$$

$$\beta_{1d} = \frac{4\gamma_e^2 k^2 P_{2x0} L}{r^2 \overline{n}_2 \rho_0 c v \Gamma_B} \cdot \frac{1}{2} \frac{1 + \mathbf{S}_{y1} \cdot \mathbf{S}_{x2}}{1 + \left(\xi_{yx}^{SW}\right)^2}, \tag{16}$$

$$\beta_{2a} = \frac{4\gamma_e^2 k^2 P_{3x0} L}{r^2 \overline{n}_3 \rho_0 c v \Gamma_B} \cdot \frac{1}{2} \frac{1 + \mathbf{S}_{x1} \cdot \mathbf{S}_{x3}}{1 + \left(\xi_{xx}^{ASW}\right)^2}, \tag{17}$$

$$\beta_{2b} = \frac{4\gamma_e^2 k^2 P_{3y0} L}{r^2 \overline{n}_3 \rho_0 c v \Gamma_B} \cdot \frac{1}{2} \frac{1 + \mathbf{S}_{x1} \cdot \mathbf{S}_{y3}}{1 + \left(\xi_{xy}^{ASW}\right)^2}, \tag{18}$$

$$\beta_{2c} = \frac{4\gamma_e^2 k^2 P_{3y0} L}{r^2 \overline{n}_3 \rho_0 c v \Gamma_B} \cdot \frac{1}{2} \frac{1 + \mathbf{S}_{y1} \cdot \mathbf{S}_{y3}}{1 + \left(\xi_{yy}^{ASW}\right)^2}, \tag{19}$$

$$\beta_{2d} = \frac{4\gamma_e^2 k^2 P_{3x0} L}{r^2 \overline{n}_3 \rho_0 c v \Gamma_B} \cdot \frac{1}{2} \frac{1 + \mathbf{S}_{y1} \cdot \mathbf{S}_{x3}}{1 + \left(\xi_{yx}^{ASW}\right)^2}, \tag{20}$$

$$\beta_{3a} = \frac{4\gamma_e^2 k^2 P_{1x0} L}{r^2 \overline{n}_1 \rho_0 c v \Gamma_B} \left(\frac{\omega_2}{\omega_1}\right)^2 \cdot \frac{1}{2} \frac{1 + \mathbf{S}_{x1} \cdot \mathbf{S}_{x2}}{1 + \left(\xi_{xx}^{SW}\right)^2}, \tag{21}$$

$$\beta_{3b} = \frac{4\gamma_e^2 k^2 P_{1y0} L}{r^2 \overline{n}_1 \rho_0 c v \Gamma_B} \left(\frac{\omega_2}{\omega_1}\right)^2 \cdot \frac{1}{2} \frac{1 + \mathbf{S}_{y1} \cdot \mathbf{S}_{x2}}{1 + \left(\xi_{yx}^{SW}\right)^2} \tag{22}$$

$$\beta_{3c} = \frac{4\gamma_e^2 k^2 P_{1y0} L}{r^2 \overline{n}_1 \rho_0 c v \Gamma_B} \left(\frac{\omega_2}{\omega_1}\right)^2 \cdot \frac{1}{2} \frac{1 + \mathbf{S}_{y1} \cdot \mathbf{S}_{y2}}{1 + \left(\xi_{yy}^{SW}\right)^2}, \tag{23}$$

$$\beta_{3d} = \frac{4\gamma_e^2 k^2 P_{1x0} L}{r^2 \overline{n}_1 \rho_0 c v \Gamma_B} \left(\frac{\omega_2}{\omega_1}\right)^2 \cdot \frac{1}{2} \frac{1 + \mathbf{S}_{x1} \cdot \mathbf{S}_{y2}}{1 + \left(\xi_{xy}^{\mathrm{SW}}\right)^2}, \tag{24}$$

$$\beta_{4a} = \frac{4\gamma_e^2 k^2 P_{1x0} L}{r^2 \overline{n}_1 \rho_0 c v \Gamma_B} \left(\frac{\omega_3}{\omega_1}\right)^2 \cdot \frac{1}{2} \frac{1 + \mathbf{S}_{x1} \cdot \mathbf{S}_{x3}}{1 + \left(\xi_{xx}^{\mathrm{ASW}}\right)^2}, \tag{25}$$

$$\beta_{4b} = \frac{4\gamma_e^2 k^2 P_{1y0} L}{r^2 \overline{n}_1 \rho_0 c v \Gamma_B} \left(\frac{\omega_3}{\omega_1}\right)^2 \cdot \frac{1}{2} \frac{1 + \mathbf{S}_{y1} \cdot \mathbf{S}_{x3}}{1 + \left(\xi_{yx}^{\mathrm{ASW}}\right)^2}, \tag{26}$$

$$\beta_{4c} = \frac{4\gamma_e^2 k^2 P_{1y0} L}{r^2 \overline{n}_1 \rho_0 c v \Gamma_B} \left(\frac{\omega_3}{\omega_1}\right)^2 \cdot \frac{1}{2} \frac{1 + \mathbf{S}_{y1} \cdot \mathbf{S}_{y3}}{1 + \left(\xi_{yy}^{\mathrm{ASW}}\right)^2}, \tag{27}$$

$$\beta_{4d} = \frac{4\gamma_e^2 k^2 P_{1x0} L}{r^2 \overline{n}_1 \rho_0 c v \Gamma_B} \left(\frac{\omega_3}{\omega_1}\right)^2 \cdot \frac{1}{2} \frac{1 + \mathbf{S}_{x1} \cdot \mathbf{S}_{y3}}{1 + \left(\xi_{xy}^{\mathrm{ASW}}\right)^2}. \tag{28}$$

The change of variables u and v transforms the system of Eqs. (1)—(6) of counter-propagating waves into the system of Eqs. (7)–(12) of co-propagating waves, where k is the wavevector and r is the radius of the fiber. Consequently, we are able to set the initial condition as $Y_{ij0}(t,0) = \left[\tanh\left(a_1(t-b_1)\right)\right] \cdot \left[\tanh\left(-a_2(t-b_2)\right)\right] + 1$, each of which takes place at the same end of the new coordinate system, where i = 1, 2, 3 and $j = x, y$. The parameters a_1 and a_2 determine the rise time of the PW, SW, and ASW pulse profiles, whereas the parameters b_1 and b_2 define the center of the pulses via the expression $/b_2 - b_1/\!/2$.

Although there exist many numerical methods of solution for SBS equations[20,21], the sixth-order Runge-Kutta method was used to numerically solve the system of Eqs. (7)–(12), and was chosen for its stability and relatively large step size[22].

Output spectra were calculated by detuning the Stokes and anti-Stokes frequencies, ω_2 and ω_3, synchronously, as done in the typical experimental setup[6,7,23]. Output powers were calculated as $P_{ij\text{-out}} = P_{ij0}\, Y_{ij\text{-out}}$, i = 1, 2, 3, and $j = x, y$, and the total power of the PW, SW, and ASW was calculated to be $P_i = P_{ix} + P_{iy}$, i = 1, 2, 3. Also, the attenuation in the fiber has been approximated as $\alpha_{ij} = \alpha$ = 0.2 dB/km, i = 1, 2, 3 , and $j = x, y$, which is a valid simplification for short fiber lengths, such as the one used in this work. The following parameters of the fiber were used: n_{avg} = 1.45, r = 4.1 μm, γ_e = 0.902, λ = 1550 nm, ρ_0 = 2.21 g/cm^3, v = 5616 m/s, L = 45 m, and Γ_B = 0.1 GHz.

For sensing applications such as the ODPA-BOTDA systems[10,11], the pump and pulse powers are chosen to be relatively low, with $P_{\mathrm{pump}} > P_{\mathrm{pulse}}$. In addition, the ODPA system functions ideally when the SW and ASW are balanced, causing the gain and loss to eliminate each other, creating a "similar" effect to the subtraction process in the differential pulse–width pair BOTDA in the electric domain. For this reason, for the simulations performed in this letter, the PW was given a power of $P_{1x} = P_{1y}$ = 1 mW, whereas the SW and ASW were given increasing powers from $P_{2x} = P_{2y} = P_{3x} = P_{3y}$ = 0.1 to 0.9 mW in nine different simulations. Elliptical birefringences of $\Delta n = 10^{-4}$, 10^{-5}, and 10^{-6} were investigated, and compared with the case of negligible birefringence, $\Delta n = 10^{-10}$. A random elliptical polarization is assigned to the pulses, having a Stokes vector $\mathbf{S}$ = (0.1, 0.9, 0.424)[14]. A pulse length of 7.5 ns has been chosen for the SW and ASW, respectively, and the resolution of the detuning axis is about 1 MHz.

Here the gain dominant regime is investigated. Pulse powers have been chosen to be between 0.1 and 0.6 mW. As can be seen from Fig. 2, the output pump spectra look substantially Lorentzian, since for the powers chosen, the combined Brillouin gain and loss operates in the gain dominant regime. With increases in pulse powers from 0.1 to 0.6 mW, the Brillouin spectrum becomes increasingly distorted. This is caused by an imbalance between the gain and loss processes, since the regime is gain dominant, the loss experienced by the PW contributes in creating an asymmetry in the output pump spectra.

In addition to the contributing gain and loss processes, birefringence of the optical fiber causes the appearance of fast and slow axes, which results in two optical modes in the fiber with different SBS frequency shifts. This causes a mismatch in the corresponding momentum vectors of the acoustic waves, thereby making it impossible for both principal axes to be resonant with the acoustic phonons. The mismatch in phonon resonance causes a Brillouin shift, $\Delta\upsilon_B$.

For each power distribution, the spectral shift was calculated for each degree of birefringence (Fig. 3(A)).

It is apparent from Fig. 3(A) that the degree of birefringence has a nonlinear effect on the Brillouin shift $\Delta\upsilon_B$. In particular, the larger the birefringence, the larger the shift, regardless of the power distribution. This spectral shift can in turn be used to quantify the birefringence of the optical fiber upon measurement of the output signal. Understandably, the largest shifts occur for the smallest power disparity between the pump and pulses, whereas the smallest shift occurs for the largest power disparity, since the case of smaller power disparity (Fig. 2(f)), yields a greater spectral distortion due to a stronger competing gain and loss process, whereas the spectral distortion of Fig. 2(a) is nearly noticeable.

To assess the effect of birefringence on the asymmetry of the output spectral, the spectral width at half-maximum on the left, $\Delta\upsilon_L$, and the spectral width at half-maximum on the right, $\Delta\upsilon_R$, were measured and their ratio = $\Delta\upsilon_L/\Delta\upsilon_R$ was calculated. Exemplary $\Delta\upsilon_L$ and $\Delta\upsilon_R$ are shown in Fig. 2(f) for clarity, a perfectly symmetric spectrum would have a ratio = 1. Figure 3(B) shows the ratios for the different power distributions, as well as for different Δn, from which it is confirmed that an increase in pulse power increases the

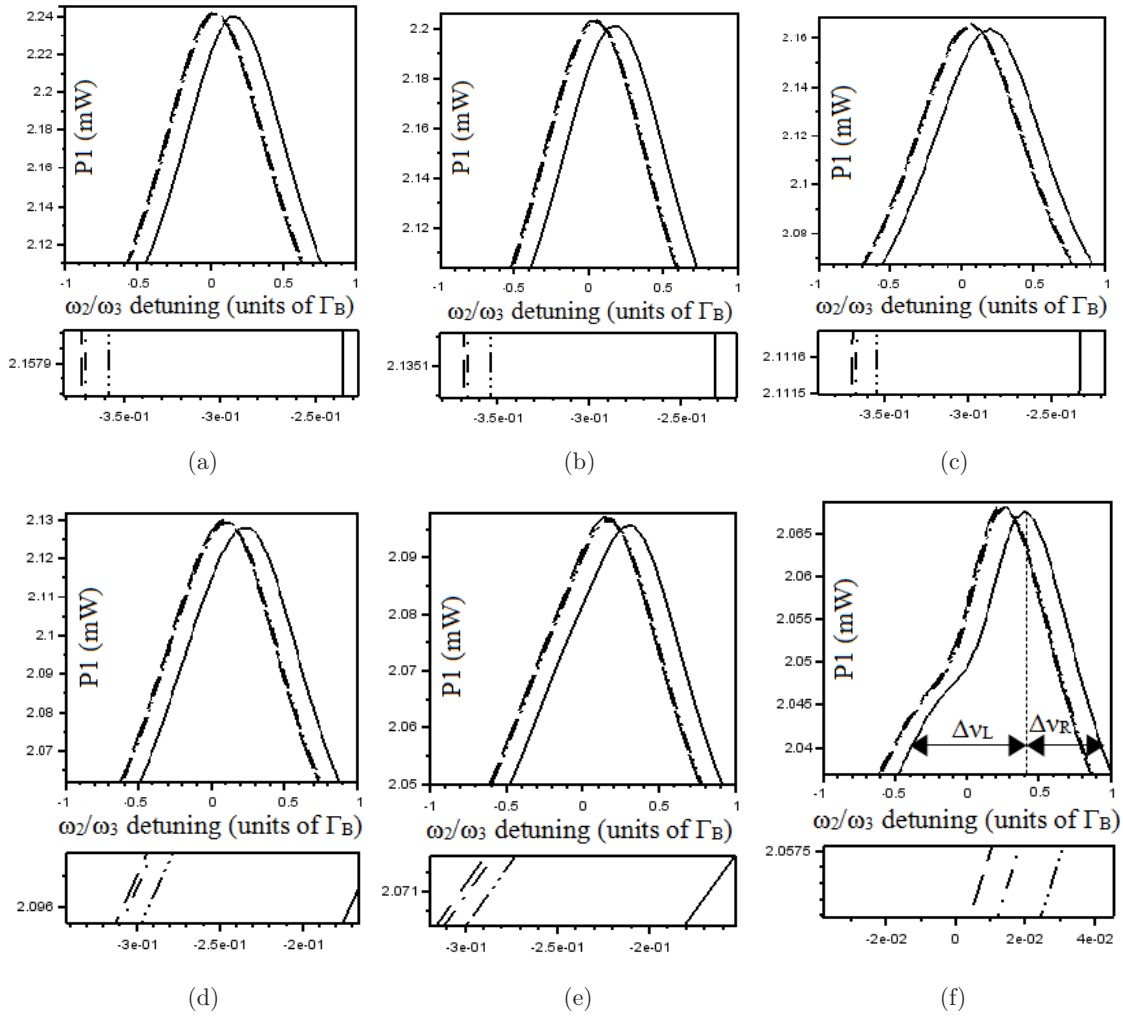

Fig. 2. Output pump spectra. **S** = (0.1, 0.9, and 0.42), L = 45 m, $P_{1x} = P_{1y}$ = 1 mW. (a) $P_{2x} = P_{2y} = P_{3x} = P_{3y}$ = 0.1 mW, (b) $P_{2x} = P_{2y} = P_{3x} = P_{3y}$ = 0.2 mW, (c) $P_{2x} = P_{2y} = P_{3x} = P_{3y}$ = 0.3 mW, (d) $P_{2x} = P_{2y} = P_{3x} = P_{3y}$ = 0.4 mW, (e) $P_{2x} = P_{2y} = P_{3x} = P_{3y}$ = 0.5 mW, and (f) $P_{2x} = P_{2y} = P_{3x} = P_{3y}$ = 0.6 mW. ——, $\Delta n = 10^{-4}$; —••—••—, $\Delta n = 10^{-5}$; —•—•—, $\Delta n = 10^{-6}$; — — —, $\Delta n = 10^{-10}$ **S** = (0, 0, 0).

spectral distortion (asymmetry) of the output plots. Although the general asymmetrical shape is a result of the competing gain and loss processes, an increase in birefringence contributes to the asymmetry, increasing the disparity between $\Delta\upsilon_L$ and $\Delta\upsilon_R$, as seen by the increase in the ratio, as compared with the case of negligible birefringence, $\Delta n = 10^{-10}$ with Stokes vector **S** = (0, 0, 0), which has been taken to be a first-order approximation to truly unpolarized light.

In the most general case of elliptical birefringence, there are four running acoustic waves, each having its own resonance frequency. As a result, each of the

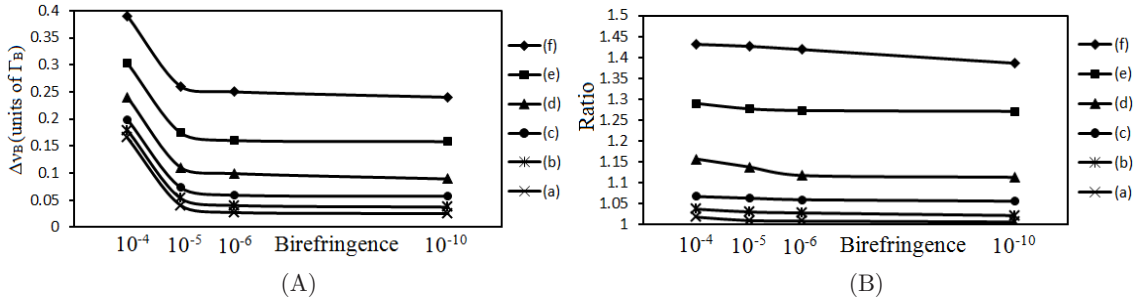

Fig. 3 (A) $\Delta\upsilon_B$ dependence on Δn. (B) ratio dependence on Δn. L = 45 m, **S** = (0.1, 0.9, and 0.42). (a) $P_2 = P_{2y} = P_{3x} = P_{3y}$ = 0.1 mW, (b) $P_{2x} = P_{2y} = P_{3x} = P_{3y}$ = 0.2 mW, (c) $P_{2x} = P_{2y} = P_{3x} = P_{3y}$ = 0.3 mW, (d) $P_{2x} = P_{2y} = P_{3x} = P_{3y}$ = 0.4 mW, (e) $P_{2x} = P_{2y} = P_{3x} = P_{3y}$ = 0.5 mW, and (f) $P_{2x} = P_{2y} = P_{3x} = P_{3y}$ = 0.6 mW.

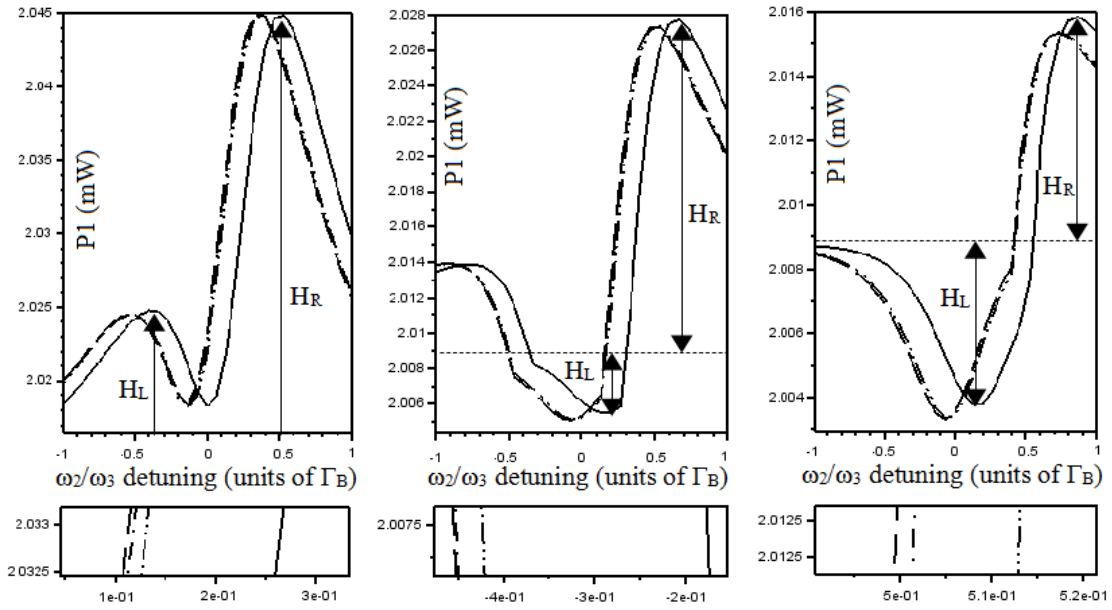

Fig. 4. Output pump spectra. **S** = (0.1, 0.9, 0.42), L = 45 m, $P_{1x} = P_{1y}$ = 1 mW. (a) $P_{1x} = P_{2y} = P_{3x} = P_{3y}$ = 0.7 mW, (b) $P_{2x} = P_{2y} = P_{3x} = P_{3y}$ = 0.8 mW, and (c) $P_{2x} = P_{2y} = P_{3x} = P_{3y}$ = 0.9 mW. ——, $\Delta n = 10^{-4}$; —••—••, $\Delta n = 10^{-5}$; —•—•—, $\Delta n = 10^{-6}$; — — —, $\Delta n = 10^{-10}$ **S** = (0, 0, 0).

fast and slow modes has its own resonant frequency at which energy transfer occurs. The result is an asymmetric spectral shape due to the uneven energy transfer along different resonant frequencies. The effects of PMD contribute to the spectral distortion seen in Fig. 3(B), since the existence of fast and slow axes causes the two optical modes to travel at different speeds, and arrive at the end of the fiber at differing times[14]. This often causes a spectral spreading, and in combination with the multiple resonance frequencies can account for the increase in distortion.

Although the gain and loss processes were competing as shown earlier, due to the power distributions chosen, the regime was mainly gain dominant. For higher pulse powers, the loss process becomes stronger, making the effects of the gain and loss regime comparable. Here the competing gain and loss regime are investigated. Pulse powers were increased from 0.7 to 0.9 mW.

As can be seen from Fig. 4, the comparable gain and loss processes substantially alter the output pump spectrum from its previous Lorentzian shape[7,15]. In Fig. 4(a), the result is dual peaks, whereas in Figs. 4(b) and (c), there is a simultaneous gain and loss spectra. A spectral shift is still apparent, in Fig. 4(a), the positions of the two peaks have been measured, whereas in Figs. 4(b) and (c) the positions of the peaks and troughs have been measured. The results are shown in Fig. 5(A), where the same general trend is observed as in Fig. 3(A).

Similar to the analysis of the gain dominant regime, to assess the effect of birefringence on the asymmetry of the output spectra, the disparity between peak heights for various degrees of birefringence was measured. Namely for Fig. 4(a), the height of the peak on the left, H_L and the height of the peak on the right, H_R, were measured and their ratio = H_L/H_R was calculated. For Figs. 4(b) and (c), the dip of the peak on the left, H_L and the height of the peak on the right, H_R, were measured, and their ratio = H_L/H_R was calculated. The H_L and H_R for each case is shown in Fig. 4. Figure 5(B) shows the ratios for different Δn, for the case of spectral burning depicted in Fig. 4(a), whereas Fig. 5(C) shows the ratios for the different power distributions and different Δn for the case of simultaneous gain and loss depicted in Figs. 4(b) and (c). Similar to the above mentioned, a perfectly symmetric spectrum can have a ratio = 1.

The dual peak effect of Fig. 4(a) can be explained as a result of a sufficiently strong loss process, which causes a portion of the pump spectra to become substantially depleted, but not sufficiently strong enough to create a lossy spectrum. It can be seen from Fig. 5(A) that the disparity between the heights of the peaks increases with increasing birefringence, represented by the decreasing ratio, birefringence contributes once again to spectral asymmetry.

However, looking at Fig. 5(C), it is apparent that with increasing birefringence, the disparity between the gain and loss peaks decreases, represented by the ratio becoming closer to 1, hence the asymmetry decreases. This can be explained by the same multiple resonant frequency argument as was used earlier. The same energy transfer that contributed to the increase in spectral asymmetry in the gain dominant regime now

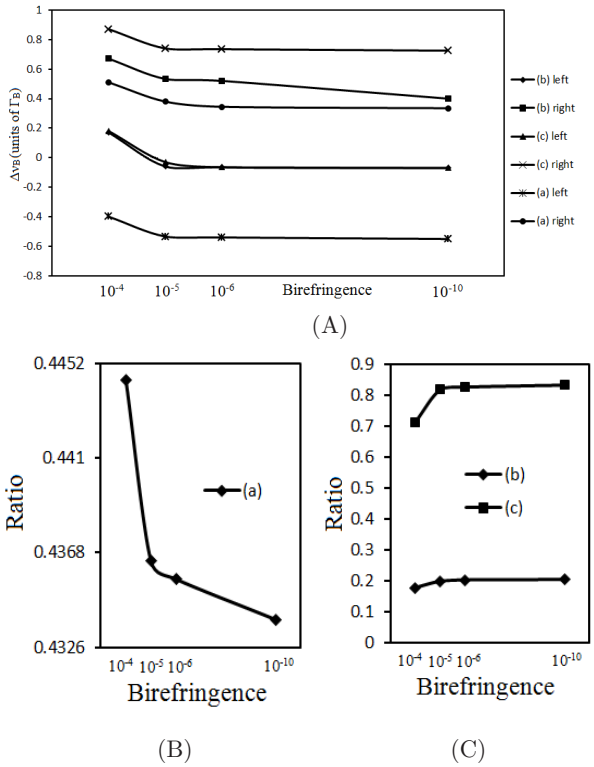

Fig. 5. (A) Δv_B dependence on Δn. (B) and (C) ratio dependence on Δn. L = 45 m, **S** = (0.1, 0.9, and 0.42). (a) $P_{2x} = P_{2y} = P_{3x} = P_{3y} = 0.7$ mW, (b) $P_{2x} = P_{2y} = P_{3x} = P_{3y} = 0.8$ mW, and (c) $P_{2x} = P_{2y} = P_{3x} = P_{3y} = 0.9$ mW.

contributes to creating a more symmetrical simultaneous gain and loss spectra in Figs. 4(b) and (c).

As can be seen from Figs. 2 and 4, the effects of PMD and PDL caused by birefringence result in a spectral distortion effect, similar to the one reported in Refs. [7,14] for BOTDA systems. Since elliptical polarizations of the interacting pulses include vertical, horizontal, and circular components in their Stokes vectors, it is therefore expected that the resulting gain can be different from the case of parallel linear alignment, where both waves have the Stokes vector (1, 0, 0) and experience maximum gain along one resonant frequency[3,12,24]. In the case of elliptical polarization, wherein there exists an interaction along all components of the Poincaré sphere, an increase in distortion effects is expected, as compared with the case of perfectly parallel polarized light, often attributed to models of Brillouin gain and loss which do not account for polarization[6,10,11,25,26]. In the gain dominant regime, this distortion contributes to the asymmetry of the output pump spectrum and conversely in the competing gain and loss regime, the distortion contributes to making the output spectra more symmetrical.

The spectral distortion effect is highly detrimental for the ODPA-BOTDA sensor system employing Lorentzian spectra[10,11], where an inaccurate spectral reading can cause inaccuracies in the operation of the sensor. Based on the results of this letter, it is therefore beneficial to choose powers in the gain dominant regime. Not only is the output pump spectrum substantially Lorentzian in this regime, but the higher the disparity in power between the pump and pulses, the more minimal the effect of birefringence is on the spectral distortion of the output pulse.

In conclusion, the most general model of elliptical birefringence in an optical fiber is extended to describe a transient Brillouin interaction including both gain and loss. We investigate spectral distortion effects related to birefringence in the gain dominant and competing gain and loss regimes. It is shown that the spectral distortion caused by birefringence can be minimized by choosing pump and pulse powers with a large disparity.

This work was financially supported by the NSERC Discovery Grants and the Canada Research Chair Program.

References

1. R. Boyd, *Nonlinear Optics* (Academic Press, 1992).
2. G. P. Agrawal, *Nonlinear Fiber Optics* (Academic Press, 2006).
3. R. H. Stolen, J. Quant. Electron. **QE-15,** 1157 (1979).
4. D. R. Walker, M. Bashkanski, A. Gulian, F. K. Fatemi, and M. Steiner, JOSA B **25,** C61 (2008).
5. O. Shlomovits and M. Tur, Opt. Lett. **38,** 836 (2013).
6. X. Bao and L. Chen, Sensors **11,** 4152 (2011).
7. S. Xie, M. Pang, X. Bao, and L. Chen, Opt. Express **20,** 6385 (2012).
8. F. Ravet, *Performance of the Distributed Brillouin Sensor: Benefits and Penalties Due to Pump Depletion* (University of Ottawa Press, 2007).
9. T. Horiguchi, K. Shimizu, T. Kurashima, M. Tateda, and Y. Koyamada, J. Lightw. Technol. **13,** 1296 (1995).
10. Y. Li, X. Bao, Y. Dong, and L. Chen, J. Lightw. Technol. **28,** 2621 (2010).
11. X. Bao and L. Chen, Photon. Sens. **1,** 102 (2011).
12. L. Ursini, M. Santagiustina, and L. Palmieri, IEEE Photon. Technol. Lett. **22,** 712 (2010).
13. W. Zou, Z. He, and K. Hotate, Opt. Express **17,** 1248 (2009).
14. D. Williams, X. Bao, and L. Chen, Photon. Res. **2,** 1 (2014).
15. A. Zadok, S. Chin, L. Thevenaz, E. Zilka, A. Eyal, and M. Tur, Opt. Lett. **34,** 2530 (2009).
16. E. Collette, *Field Guide to Polarization* (SPIE Press, 2005).
17. A. Kumar and A. Ghatak, *Polarization of Light with Applications in Optical Fibers* (SPIE Press, 2011).
18. D. Williams, X. Bao, and L. Chen, Photon. Res. **2,** 126 (2014).
19. L. Chen and X. Bao, Opt. Commun. **152,** 65 (1998).
20. J. W. D. Chi, L. Chao, and M. K. Rao, J. Quant. Electron. **37,** 1329 (2001).
21. R. Chu, M. Kanefsky, and J. Falk, J. Appl. Phys. **71,** 4653 (1992).
22. H. A. Luther, Math. Comput. **22,** 424 (1968).
23. W. Zou, C. Jin, and J. Chen, Appl. Phys. Express **5,** 082503 (2012).
24. M. O. V. Deventer and A. J. Boot, J. Lightw. Technol. **12,** 585 (1994).
25. D. Williams, X. Bao, and L. Chen, Appl. Opt. **52,** 3404 (2013).
26. D. Williams, X. Bao, and L. Chen, Chin. Opt. Lett. **12,** 082001 (2014).